Global optimization of neutral and charged 20- and 55-atom silver and gold clusters at the DFTB level

Nathalie Tarrat, Mathias Rapacioli, Jérôme Cuny, Joseph Morillo, Jean-Louis Heully, Fernand Spiegelman

Global Optimization of Neutral and Charged 20- and 55-Atom Silver and Gold Clusters at the DFTB Level

Nathalie Tarrat[a,*], Mathias Rapacioli[b,*], Jérôme Cuny[b], Joseph Morillo[a,c], Jean-Louis Heully[b], Fernand Spiegelman[b]

[a] *CEMES-CNRS UPR 8011, 29 rue Jeanne Marvig, BP 94347, 31055 Toulouse Cedex 4, France*
[b] *Laboratoire de Chimie et Physique Quantiques LCPQ/IRSAMC, UMR5626, Université de Toulouse (UPS) and CNRS, 118 Route de Narbonne, F-31062 Toulouse, France*
[c] *Université de Toulouse(UPS), 118 Route de Narbonne, F-31062 Toulouse Cedex 9, France*

Abstract

The global optimization of metallic clusters is an important topic because nanoclusters exhibit structure-dependent properties. In this paper, we present a global optimization study of Ag_{20}, Au_{20}, Ag_{55} and Au_{55} in their neutral and charge states (-1, 0, +1) conducted using a Parallel-Tempering Molecular Dynamics algorithm at the DFTB level without pre-screening. For Au_{20}, Ag_{20} and their ions, the present DFTB low energy structures are in good agreement with previously published calculations and experimental data. In the case of Ag_{55}^- and Au_{55}^-, the present study is consistent with photo-electron detachment experiments suggesting highly symmetric icosahedral structures for silver and more disordered morphologies for gold. The present results are also compatible with trapped ion electron diffraction experiments and calculations for Ag_{55}^+ and Ag_{55}^-. We report low-energy isomers of Au_{55} exhibiting cavities below their external shell. This work quantitatively confirms the relevance of DFTB for structure calculation of noble metal clusters. Furthermore, it also demonstrates the feasibility of global optimization using DFTB, without pre-screening through classical potential, for sizes up to a few tens of atoms and for different charge states.

*Corresponding authors
Email addresses: nathalie.tarrat@cemes.fr (Nathalie Tarrat), mathias.rapacioli@irsamc.ups-tlse.fr (Mathias Rapacioli)

Keywords: Gold, Silver, Clusters, Global Optimization, DFTB

1. Introduction

The prediction of the atomic structure of nanoclusters is of fundamental importance as they often exhibit size-dependent properties. A deep knowledge of the structural changes arising as a function of the nanocluster size and charge can lead to the development of materials exhibiting desirable properties. Among nanoclusters, silver and gold ones display very specific optical [1, 2, 3, 4, 5, 6, 7, 8, 9, 10, 11, 12, 13] and chemical [14, 15, 16, 17, 18, 19, 20, 21, 22] properties. A variety of experimental and computational methods have thus been used to predict their structures in their neutral or charged states i.e. $Ag_n^{-,0,+}$ and $Au_n^{-,0,+}$ [23, 24, 25, 26, 27, 28, 29, 30, 31, 32, 33, 34, 35, 36, 37, 38, 39, 40, 41, 42, 43, 44, 45, 46, 47, 48].

Among others, the structure of noble metal clusters has now become a very topical theme with the possibility of monitoring directly their structural behaviors via STEM imaging [49]. For the medium-size silver and gold clusters with 20 and 55 atoms, the presently known structures are issued from either theoretical studies or studies coupling experimental characterization with DFT calculations [27, 28, 39, 50, 51, 52, 53]. However, to the best of our knowledge, no full DFT exploration of the potential energy surface (PES) of such clusters is mentioned in the literature. Indeed, despite fast progress in the derivation of accurate functionals and efficient algorithms to be implemented on high performance computers, DFT is not yet efficient enough to be directly used within global and extensive exploration of PES. Consequently, most global explorations in the field of structure prediction of medium-size metallic clusters use pre-screening, i.e. are performed by first exploring the energy landscapes using an empirical or a semi-empirical potential. This is followed by a subsequent optimisation of the lower-energy structures at a higher level of accuracy, generally DFT.

To study such systems with an accuracy close to that of *ab initio* meth-

ods, parameterized quantum approaches offer an attractive alternative as they preserve, with some approximations, the electronic description of the system while displaying a significantly lower computational cost. An explicit quantum description of the electronic structure is obviously desirable when one wishes to describe several charge states within a unique scheme, which is almost impossible when using classical force fields. Among the available options, the Density-Functional based Tight-Binding method (DFTB) is considered as a state-of-the-art parameterized method [54, 55, 56, 57, 58, 59]. It is derived from DFT via several approximations and has proved to be particularly efficient for the description of complex molecular systems [60, 61, 62, 63]. Its accuracy depends significantly on the quality of the parameterization. In particular, it requires the use of tabulated integrals, referred to as the Slater-Koster integrals, constructed for each atomic pair of the chemical system of interest. These Slater-Koster integrals are not uniquely defined as they can be developed using various methodologies and reference DFT functionals. In the particular case of silver and gold, several DFTB parameter sets have been proposed in the literature [64, 65, 66]. In a recent study [67], we improved such parameters for silver and gold clusters and showed that these modified parameters are satisfactory in reproducing essential differences between small silver and gold clusters. In particular, their 2D-3D structural transition and its dependency upon cluster charge state is well reproduced as well as a variety of bulk properties. Our DFTB results were also in agreement with previously reported DFT and experimental data in the medium-size regime regarding the energetic ordering of the various low-energy isomers already described in the literature. The satisfactory behavior of these parameters regarding the modeling of middle-size silver and gold clusters now provides opportunities to perform global exploration of the PES of such aggregates with an approach providing an explicit electronic structure description.

In the present work, we use a Parallel-Tempering Molecular Dynamics algorithm (PTMD) to explore the PES of Ag_n^q and Au_n^q with $n = 20, 55$ and

$q = -1, 0, +1$ computed at the DFTB level. The size regime of a few tens is particularly interesting since it provides a transition between the small size regime, where each atom and charge fluctuation matters, and the nanoparticle regime in which the global morphology may be more determinant. The target is to present a systematic and consistent study of both sizes for the various charge states. The size n=20 has been abundantly documented in both experimental and theoretical studies and can be viewed as a test case for the present scheme. Photo-electron detachment experimental data do also exist on silver and gold anions for size 55, together with trapped ion electron diffraction (TIED) data for Ag_{55} anions and cations. Both indicate an icosahedral type structure for $Ag_{55}^{+/-}$. In contrast, the most stable structures for $Au_{55}^{+/-}$ are not yet clearly established. Moreover, it is also interesting, beyond the determination of the absolute minimum structure, to provide a picture of the structures and energy distribution of the other low-energy isomers, and to rationalize their structural patterns. Indeed, these low energy isomers may be possibly observed depending on the experiments, and will likely contribute to the aggregate properties at finite temperature. The paper is organized as follows: in section 2, the DFTB method and the global exploration scheme are briefly presented. In section 3, a detailed description of the relevant isomers extracted from the global exploration is presented. In section 4, we discuss our results in the light of the previously reported structures. Conclusions and perspectives are provided in the last section.

2. Computational Details

2.1. The DFTB and SCC-DFTB Methods

DFTB [54, 55, 56, 57, 58, 59] is an approximation of DFT in its orbital formulation proposed by Hohenberg, Kohn and Sham [68, 69]. In the DFTB method: (i) the energy is derived from a Taylor series expansion of the DFT energy around a reference density, (ii) the Kohn-Sham orbitals φ_i are expanded on a set of minimal atom-centered basis, (iii) The first order expression in this basis

involves matrix elements of the overlap and Hamiltonian ($\hat{H}^0$) at the reference density, retaining only one- and two-centers terms, (iv) the zeroth-order terms are gathered in a repulsive term E^{rep} expressed through pairwise contributions. The two levels of DFTB used in this work are: the zeroth-order DFTB and the Self-Consistent-Charge DFTB with the following expressions for the total energy:

First-order DFTB

$$E^{\mathrm{DFTB}} = \sum_{\alpha,\beta\neq\alpha}^{\mathrm{atoms}} E^{\mathrm{rep}}_{\alpha\beta} + \sum_i n_i \langle\varphi_i|\hat{H}^0|\varphi_i\rangle \quad (1)$$

Second-order DFTB, referred to as SCC-DFTB (Self-Consistent-Charge-DFTB)

$$E^{\mathrm{SCC-DFTB}} = E^{\mathrm{DFTB}} + \frac{1}{2}\sum_{\alpha,\beta}^{\mathrm{atoms}} \Gamma_{\alpha\beta} q_\alpha q_\beta \quad (2)$$

where n_i is the occupation number of molecular orbital φ_i. Concerning the parameterization, $E^{\mathrm{rep}}_{\alpha\beta}$ and the non-diagonal elements of the overlap and Hamiltonian matrices in the atomic basis are tabulated from DFT calculations on atomic dimers and expressed as a function of interatomic distances. The diagonal elements of $\hat{H}^0$ are the orbital energies of the isolated atoms. In the second order formulation, which leads to a self consistent scheme, the q_α are the Mulliken atomic charges and $\Gamma_{\alpha\beta}$ is a diatomic function derived from Hubbard parameters. The DFTB hamiltonian used[67] is spanned on a valence atomic basis including explicitely nd,$(n+1)s$ and $(n+1)p$ atomic orbitals for silver ($n=4$) and gold ($n=5$), thus allowing mixing of d,s and p valence electronic character in the cluster DFTB orbitals. Its parametrization[67] was shown to correctly describe the peculiar character of gold clusters, namely the persistence of planar geometries in gold up to sizes 8-12. The spin-restricted version of DFTB was used for all calculations.

2.2. Global Optimization Scheme

The currently most used global optimization techniques include: basin hopping and derived techniques [70, 71], simulated annealing [72] and the developments concerned with ergodicity (multi-tempering, parallel-tempering in Molecular Dynamics or Monte Carlo schemes [73, 74]), genetic/evolutionary algorithms [75], and particle swarm algorithms [76]. In this work, we chose to use Parallel-Tempering Molecular Dynamics [73] (PTMD), also known as "replica exchange" algorithm, combined with periodic quenching. In the PTMD method, R replicas of the original system under investigation are subject to evolutions in the canonical ensemble at different temperatures. The high temperature evolutions are able to sample large volumes of the phase space. In contrast, the low temperature simulations allow a more detailed sampling of the low energy regions of the phase space but with the risk of being trapped in a local energy basin. PTMD achieves an improved sampling by allowing the systems at different temperatures to exchange their configurations. The conditional inclusion of higher temperature configurations in low temperature trajectories allows lowest temperature evolutions to access larger representative sets of low-temperature regions of the phase space.

In the present simulations, the PTMD scheme involved simultaneous DFTB MD runs at 60 temperatures equally distributed in the range 0-3000 K. Fragmentation was hindered by using a spherical box. The MD timestep was set to 3 fs and exchanges were attempted using the Metropolis energy criterion every 100 timesteps. A chain of 5 Nose-Hoover thermostats [77, 78] with a unique frequency of 80 cm^{-1} was used. The length of the trajectories were 3 ns (1 million PTMD steps). From each of the three MD runs at 50 K (low T), 652 K (medium T) and 3000 K (high T) of the PTMD process, over a thousand configurations equally spaced in time were selected. They were subsequently locally optimized with the SCC-DFTB conjugated gradient scheme, providing a wealth of stable structures. High temperature trajectories were considered for quenches in order to (i) ensure a better sampling of the various low-energy regions of the phase space and (ii) obtain minima higher in energy than the global minimum. This

procedure generated a bunch of low energy isomers for each cluster size, and was repeated separately for neutrals, anions and cations, in order to avoid any bias. All calculations were performed using the deMonNano code [79], in which the PTMD scheme has recently been implemented [80]. The PTMD runs were conducted with the non-SCC first-order version of DFTB, whereas the local relaxations were achieved with the SCC-DFTB scheme. This restriction should not be too drastic, since the charge levels under consideration are low (q=0,+1,-1), the systems are metal clusters and the charge fluctuations are supposed to be weak.

3. Global Optimization Results

Clusters belonging to the same structural families were gathered on the basis of three criteria: (i) the total energy of the cluster $E^{\mathrm{SCC-DFTB}}$, (ii) the three principal mass-less inertia moments I_1,I_2 and I_3, characterizing the overall shape of the cluster (namely the usual inertia moments divided by the atom mass) and (iii) the symmetry group of the cluster [81]. In order to bring to light the structural differences between some clusters, the radial atomic distribution describing the variation of the density of atoms as a function of the distance from the center of mass of the cluster was computed. To do that, the number of atoms found in concentric spheres (with radius increments of 1 Å) was counted. We also determined the coordination numbers of the atoms, defined as the number of nearest neighbors. To do so, we used a threshold distance between two atoms of 3 Å, which is relevant for both silver and gold clusters as their nearest-neighbour distances in the bulk are almost identical, 2.889 and 2.886 Å, respectively.

3.1. Global Exploration of 20-Atom Silver Clusters

The ten most stable structures identified for $Ag_{20}^{-,0,+}$ clusters are represented in Figure 2. The same compact C_3 structure is found to be the most stable for

System	n(< 1 eV)	System	n(< 1 eV)
Ag_{20}^{-}	165	Ag_{55}^{-}	6
Ag_{20}	115	Ag_{55}	7
Ag_{20}^{+}	122	Ag_{55}^{+}	14
Au_{20}^{-}	45	Au_{55}^{-}	36
Au_{20}	2	Au_{55}	35
Au_{20}^{+}	69	Au_{55}^{+}	37

Table 1: Number of isomers found below 1 eV above the global minimum for silver and gold clusters.

both the neutral and cationic form, whereas the most stable structure for Ag_{20}^{-} belong to the C_s group. We note that for the three charge states, the second most stable isomer has a very weak structural excitation energy above the global minimum (0.006, 0.119 and 0.081 eV for the anionic, neutral and cationic forms, respectively) and that more than one hundred of different structures were identified with energies lower than 1 eV above the global minimum (see Table 1, note that the numbers given in this Table are indicators of the relative complexities of the respective PES, but cannot be considered as the exact numbers of minima on the different PES since they depend on the tolerance threshold used to distinguish between isomer structures). These structures correspond to compact structures, mostly differing by the distribution of hexagonal and pentagonal cycles at the cluster surface. This explains the low level of symmetry detected for these clusters (Table 2) and that the mean inertia moments only weakly depend on the specific isomers as seen in Figure 1.

3.2. Global Exploration of 20-Atom Gold Clusters

The most stable structures found for $Au_{20}^{-,0,+}$ are close to the well-known pyramidal T_d isomer (Figure 3), possibly presenting Jahn-teller distorsion (see below for the anion case). This pyramidal form is pretty stable as the second most stable isomers lies 0.28, 0.69 and 0.34 eV above for the anion, neutral and cation, respectively. Another difference with silver clusters is the low number of

	Isomer	ΔE (eV)	I_1	I_2	I_3	Symmetry
Ag_{20}^-	1	0.000	146.6	135.6	123.7	C_s
	2	0.006	142.6	134.9	131.6	C_1
	3	0.036	151.1	139.2	120.3	C_1
	4	0.040	139.7	139.7	137.8	C_1
	5	0.052	160.2	148.3	106.1	C_s
	6	0.064	139.6	138.2	126.3	C_s
	7	0.075	147.6	136.2	125.8	C_1
	8	0.087	154.0	133.5	122.3	C_{2v}
	9	0.095	147.9	146.3	112.7	C_{2v}
	10	0.102	145.5	141.1	118.6	C_1
Ag_{20}	1	0.000	141.7	131.8	131.8	C_3
	2	0.119	139.1	139.1	134.7	C_3
	3	0.157	140.0	135.0	125.4	C_s
	4	0.186	142.2	138.3	123.1	C_1
	5	0.201	135.4	133.6	129.7	C_s
	6	0.233	143.3	133.6	127.2	C_1
	7	0.238	145.7	136.6	121.7	C_1
	8	0.259	145.5	131.3	130.4	C_1
	9	0.301	143.4	141.1	124.9	C_{2v}
	10	0.321	140.9	138.8	119.6	C_1
Ag_{20}^+	1	0.000	142.5	129.8	129.8	C_3
	2	0.081	141.0	133.3	122.7	C_s
	3	0.090	143.8	137.2	120.8	C_1
	4	0.127	135.2	132.4	127.8	C_2
	5	0.134	140.5	138.8	117.3	C_1
	6	0.139	144.0	130.5	122.5	C_1
	7	0.159	145.9	131.3	125.7	C_1
	8	0.163	147.1	129.3	129.0	C_1
	9	0.170	150.4	131.9	120.1	C_1
	10	0.174	146.0	140.0	116.5	C_1

Table 2: Energetics and principal mass-less moments of inertia (in Å^2) of Ag_{20} clusters.

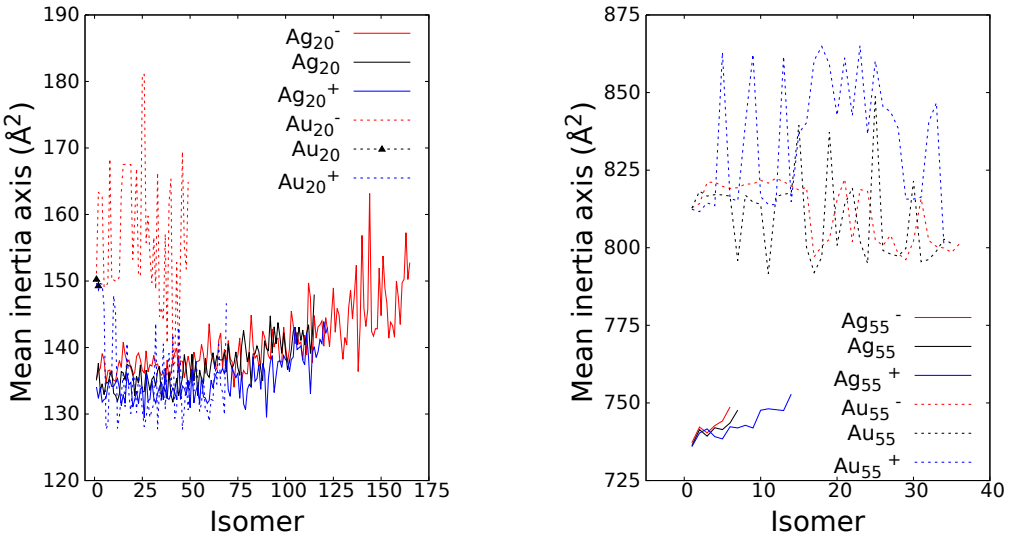

Figure 1: Mean inertia moments for silver and gold clusters of 20 (left) and 55 (right) units. On each plot, only the values of the mean inertia moments corresponding to isomers found below 1 eV above the global minimum are depicted.

structures found below 1 eV (45, 2 and 69 for the anionic, neutral and cationic states respectively, Table 1). For Au_{20}, the second most stable is a structure strongly distorted from the T_d pyramid, while third isomer can be seen as a pyramid with one apex atom displaced to the face opposite to its original position. The most stable isomer of Au_{20}^+ is also a a pyramidal structure with T_d symmetry. We have found no significant distorsion (if it exists, it is less than 0.01 Å). Many of the low energy isomers above the ground state significantly differ from the pyramidal structure. At higher energies, more compact structures are found, which explains that the mean inertia moments significantly decrease and reach values similar to those obtained for silver clusters (Figure 1). The most stable anion is also close to a T_d pyramid, however Jahn-Teller deformed towards D_{2d} (with distance distorsions of the order of 0.03 Å). The other low energy isomers differ though defects from the pyramid, namely the removal of one atom either from a face-center or an apex, transferred as an adatom on top of a triangle or of two edge atoms. In the second lowest energy isomer, the

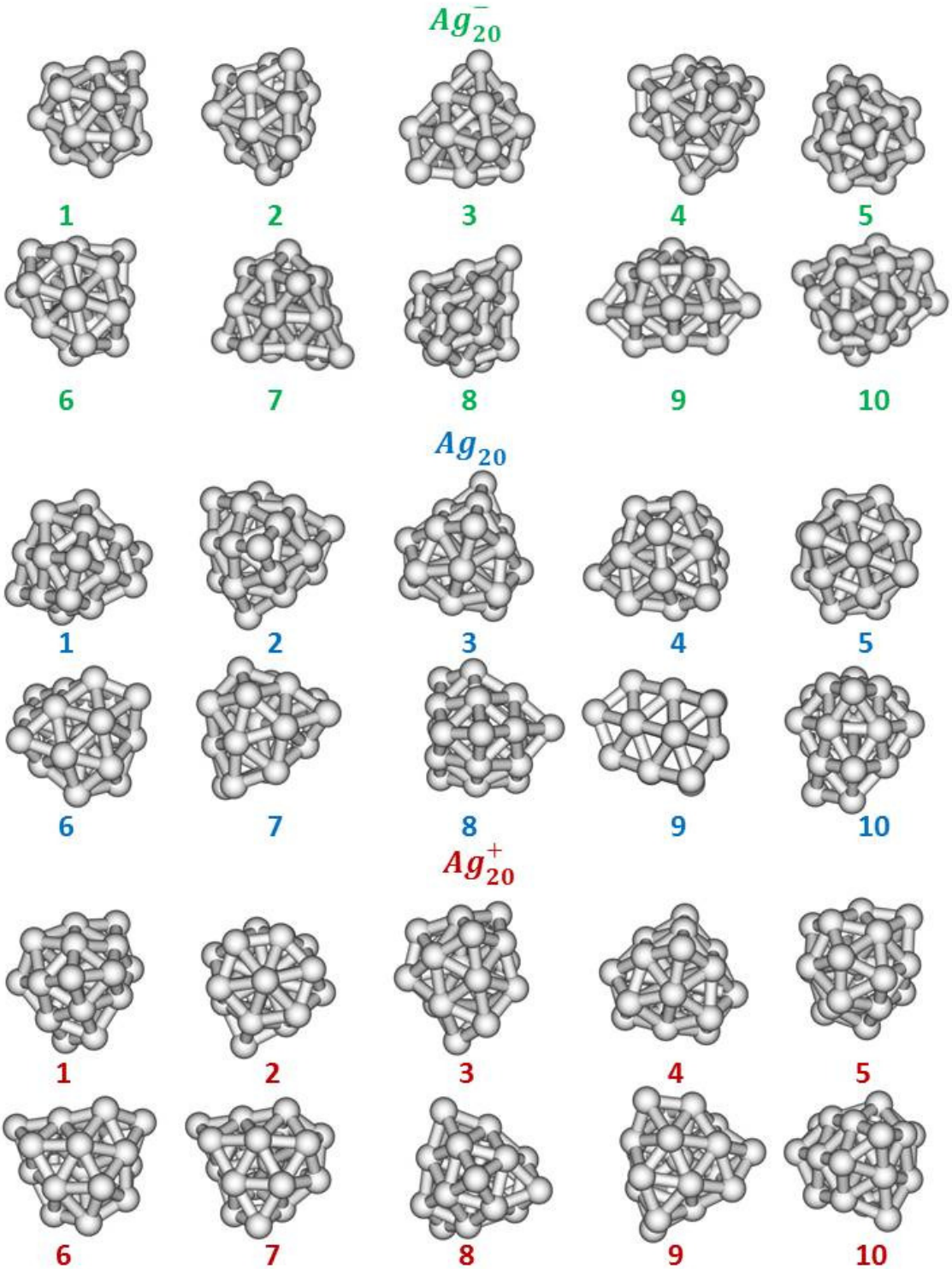

Figure 2: 10 lowest-energy minima obtained for Ag_{20}^{-} (green, top), Ag_{20} (blue, middle) and Ag_{20}^{+} (red, bottom)

removed and adatom locations correspond to the same face. When an atom is removed from a face center, it leaves a small cavity. In many structures, the removed and adatom positions belong to the same symmetry plane of the initial T_d structure, leading to C_s symmetries (Table 3). Remaining close to T_d-structures is at the origin of mean inertia moments generally larger than for the cationic forms (Figure 1).

3.3. Global Exploration of 55-Atom Silver Clusters

For the three charge states, the most stable structure found for Ag_{55} is close to an icosahedron. This icosahedron is however slightly distorted into lower symmetry deformations namely D_{3d}, D_{2h} and D_{5d} for the anion, the neutral and the cation respectively. Only 6, 7 and 14 local minima were obtained with energies lower than 1 eV above the global minimum for anionic, neutral and cationic forms, respectively (Table 1). All these optimized structures result from defects created in the icosahedron basic form, consisting of the removal of one atom on top of an hexagonal or pentagonal cycle and the addition of an atom either introduced inside a face modifying the surface constraint or added on top of a face triangle or rhombus. If the removed and adatom locations belong to the same symmetry plane, the structure is C_s and C_1 otherwise (Table 4). The structures remaining close to the icosahedron, their mean inertia moments also remain close to that of the icosahedron (Figure 1). Furthermore, very few changes are observed on the coordination numbers distributions with respect to that of the icosahedron (Figure 5). Indeed, as can be seen on this figure, the variation fluctuates mainly in the ranges 7-8 and 11-12 neighbors.

3.4. Global Exploration of 55-Atom Gold Clusters

The icosahedron form is not competitive for gold clusters with 55 units for which the most stable structure obtained present lower symmetry, quasi C_3 for the neutral, C_3 for the cation or no symmetry at all in the anion case, as can be seen in Figure 6 and Table 5 (Note that the neutral shows a very small C_1 distorsion from the C_3 structure, with deformations of the order of 0.01

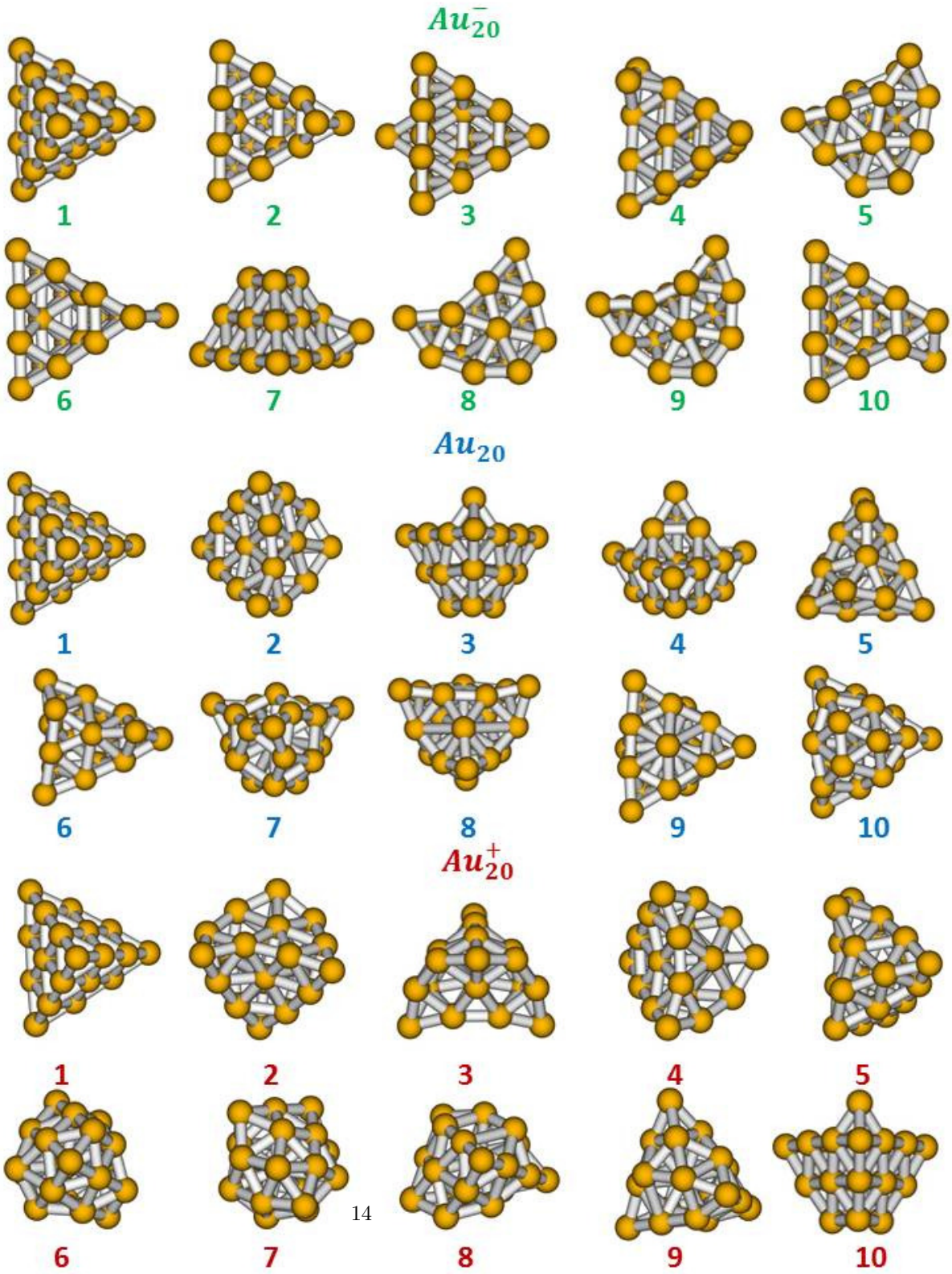

Figure 3: 10 lowest-energy minima obtained for Au_{20}^{-} (green, top), Au_{20} (blue, middle) and Au_{20}^{+} (red, bottom).

	Isomer	ΔE (eV)	I_1	I_2	I_3	Symmetry
Au_{20}^-	1	0.000	151.3	151.3	150.9	T_d (D_{2d})
	2	0.277	171.2	170.4	148.6	C_s
	3	0.361	170.2	169.1	149.2	C_1
	4	0.395	164.2	149.1	134.0	C_s
	5	0.413	162.9	149.5	137.0	C_1
	6	0.419	180.2	177.4	147.5	C_s
	7	0.423	173.8	149.8	126.7	C_1
	8	0.433	164.4	150.0	135.5	C_1
	9	0.447	164.4	151.3	136.3	C_s
	10	0.451	172.7	171.1	146.3	C_1
Au_{20}	1	0.000	150.3	150.3	150.3	T_d
	2	0.694	163.8	148.7	135.3	C_s
	3	1.010	157.1	141.0	138.5	C_s
	4	1.022	149.2	137.6	137.6	C_3
	5	1.060	165.6	140.1	134.0	C_1
	6	1.086	164.9	139.4	134.0	C_1
	7	1.183	154.4	131.1	130.8	C_1
	8	1.197	148.9	139.9	124.8	C_s
	9	1.209	157.7	130.3	129.1	C_1
	10	1.213	157.4	130.5	129.2	C_3
Au_{20}^+	1	0.000	150.7	149.2	149.2	T_d
	2	0.340	165.0	147.2	133.6	C_1
	3	0.350	166.4	148.8	133.7	C_s
	4	0.371	165.1	149.1	134.4	C_s
	5	0.416	165.8	139.3	133.1	C_1
	6	0.474	136.3	123.4	123.4	C_3
	7	0.524	144.1	128.9	112.1	C_1
	8	0.547	154.7	131.0	124.2	C_1
	9	0.551	154.2	130.5	124.4	C_1
	10	0.569	163.9	146.4	133.2	C_s

Table 3: Energetics and principal mass-less moments of inertia (in Å^2) of Ag_{55} clusters. The parenthesis indicates the group corresponding to the Jahn-Teller distorsion

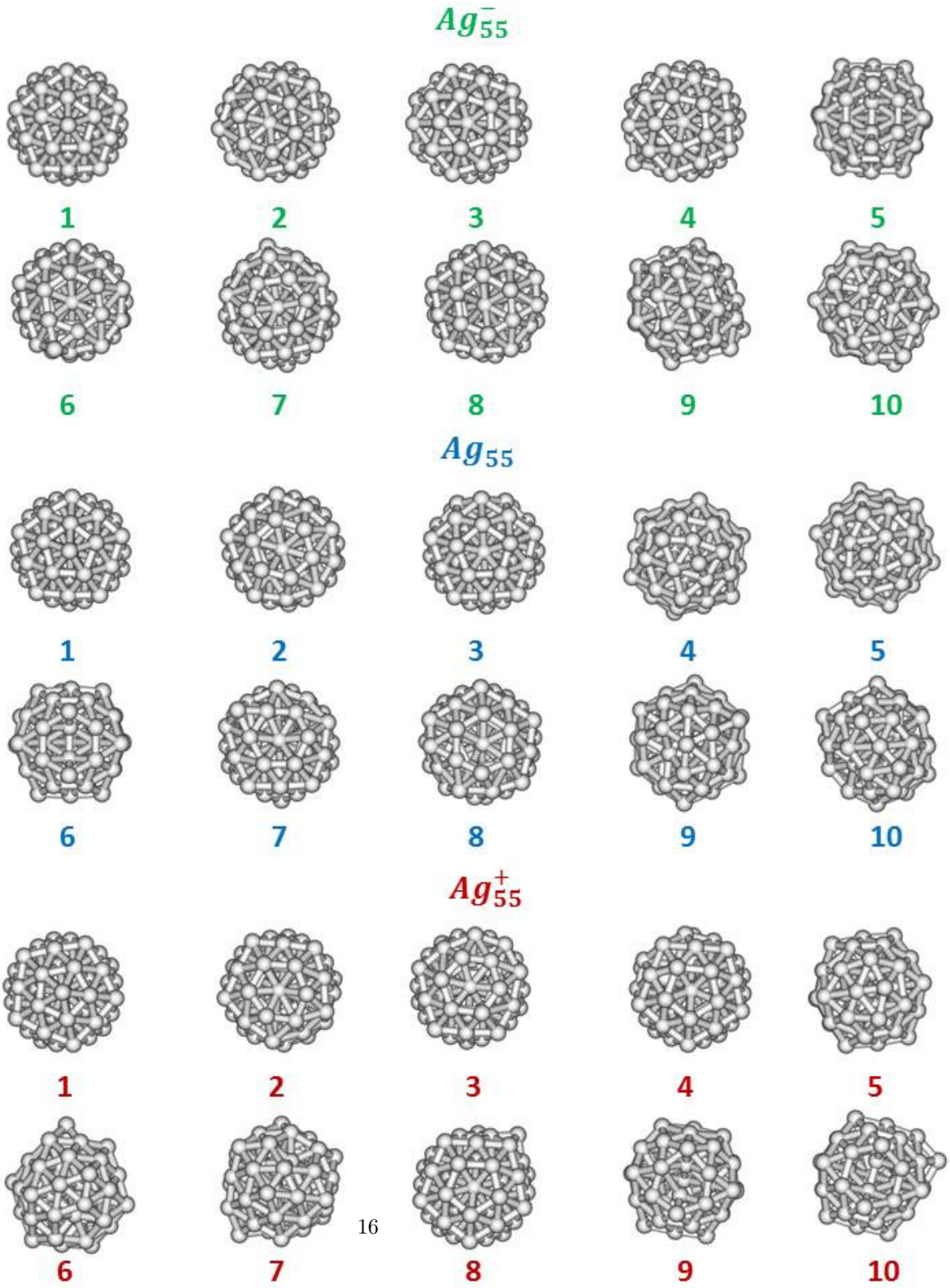

Figure 4: 10 lowest-energy minima obtained for Ag_{55}^{-} (green, top), Ag_{55} (blue, middle) and Ag_{55}^{+} (red, bottom).

	Isomer	$\Delta E(eV)$	I_1	I_2	I_3	Symmetry
Ag_{55}^-	1	0.000	743.2	734.2	734.2	I_h (D_{3d})
	2	0.501	767.9	735.3	723.5	C_s
	3	0.600	767.3	734.9	718.9	C_s
	4	0.740	778.2	736.8	713.1	C_s
	5	0.871	762.2	738.3	732.1	C_1
	6	0.964	786.6	741.0	718.6	C_1
	7	1.026	786.3	752.1	705.0	C_s
	8	1.067	802.6	728.6	714.6	C_1
	9	1.097	785.2	747.4	714.1	C_1
	10	1.136	784.0	752.0	711.3	$C1$
Ag_{55}	1	0.000	742.0	734.2	732.5	I_h (D_{2h})
	2	0.509	768.1	732.0	724.0	C_s
	3	0.599	766.0	731.1	720.8	C_s
	4	0.701	764.3	745.8	715.9	C_1
	5	0.732	760.7	739.3	724.3	C_s
	6	0.843	764.9	735.9	729.9	C_1
	7	0.950	784.5	743.5	715.0	C_1
	8	1.018	801.6	728.7	712.5	C_1
	9	1.048	785.9	753.6	706.8	C_1
	10	1.078	792.2	732.5	718.5	C_1
Ag_{55}^+	1	0.000	739.9	739.8	728.0	I_h (D_{5d})
	2	0.509	768.1	729.1	723.7	C_1
	3	0.553	767.2	741.2	716.6	C_s
	4	0.596	766.5	727.5	723.5	C_s
	5	0.632	763.0	727.3	725.0	C_s
	6	0.675	764.3	749.5	713.1	C_1
	7	0.702	766.8	740.7	718.4	C_1
	8	0.733	780.9	743.9	703.6	C_s
	9	0.783	758.9	736.6	730.2	C_s
	10	0.821	778.4	750.8	713.7	C_1

Table 4: Energetics and principal mass-less moments of inertia (in $Å^2$) of Ag_{55} clusters. The parenthesis indicates the group corresponding to the Jahn-Teller distorsion

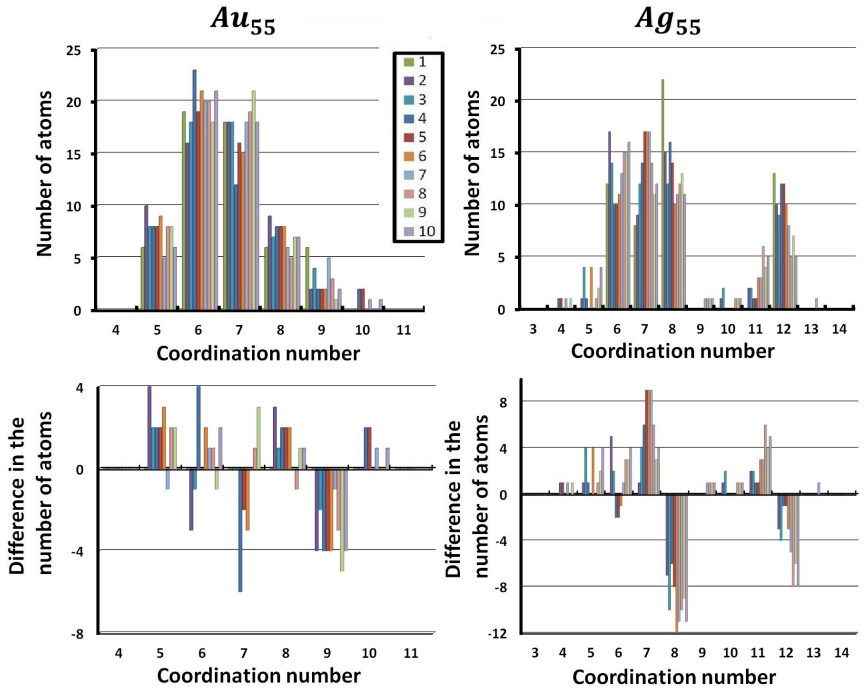

Figure 5: Top: Cumulated distributions of the coordination numbers of the atoms belonging to the top ten Au_{55} (left) and Ag_{55} (right) isomers, respectively. Bottom: Differences in the distribution of the coordination numbers with respect to the corresponding global minima.

Å). About 35 different isomers were identified with energies lower than 1 eV above that of the global minimum whatever the considered charge state (Table 1). Several patterns common to all charge states are observed. The first one is the trend to form a cavity inside the cluster as can be seen in Figure 7. The structures are therefore less compact than in the case of Ag_{55} clusters, which results in larger values of the mean inertia moments (Figure 1). The presence of these cavities can also be highlighted by comparing the radial atomic distribution of these clusters to the one of the compact icosahedron (Figure 8). The first atomic layer of the cluster is deserted, benefiting to the surface layer. We also recognized the formation of planar patterns at the surface and sometimes inside the clusters, for instance as separating walls between inside cavities. This trend can be related to the preference for 2D structures in small gold clusters, previously observed at the DFT [46] and DFTB [65, 67] levels and attributed to relativistic effects [82]. Finally, we observed that the inside separating plane is sometimes replaced by a central pillar (Figure 7), which in some cases is a C_3 symmetry axis as for instance in the most stable structures of cationic and neutral forms. Note however that most of the isomers do not present any symmetry. The variations of the coordination number distributions with respect to those of the global minima have an amplitude much smaller than in the case of silver. The most frequently observed variation is a significant reduction in the number of atoms having 9 nearest neighbors. Indeed, in the global minima, 6 atoms correspond to the two bases of the central pillar (2x3 atoms) and the loss of the C_3 symmetry induces a change in the coordination sphere of these atoms. Finally, we also report the presence of square patterns located on the clusters surfaces as can be seen in Figure 6.

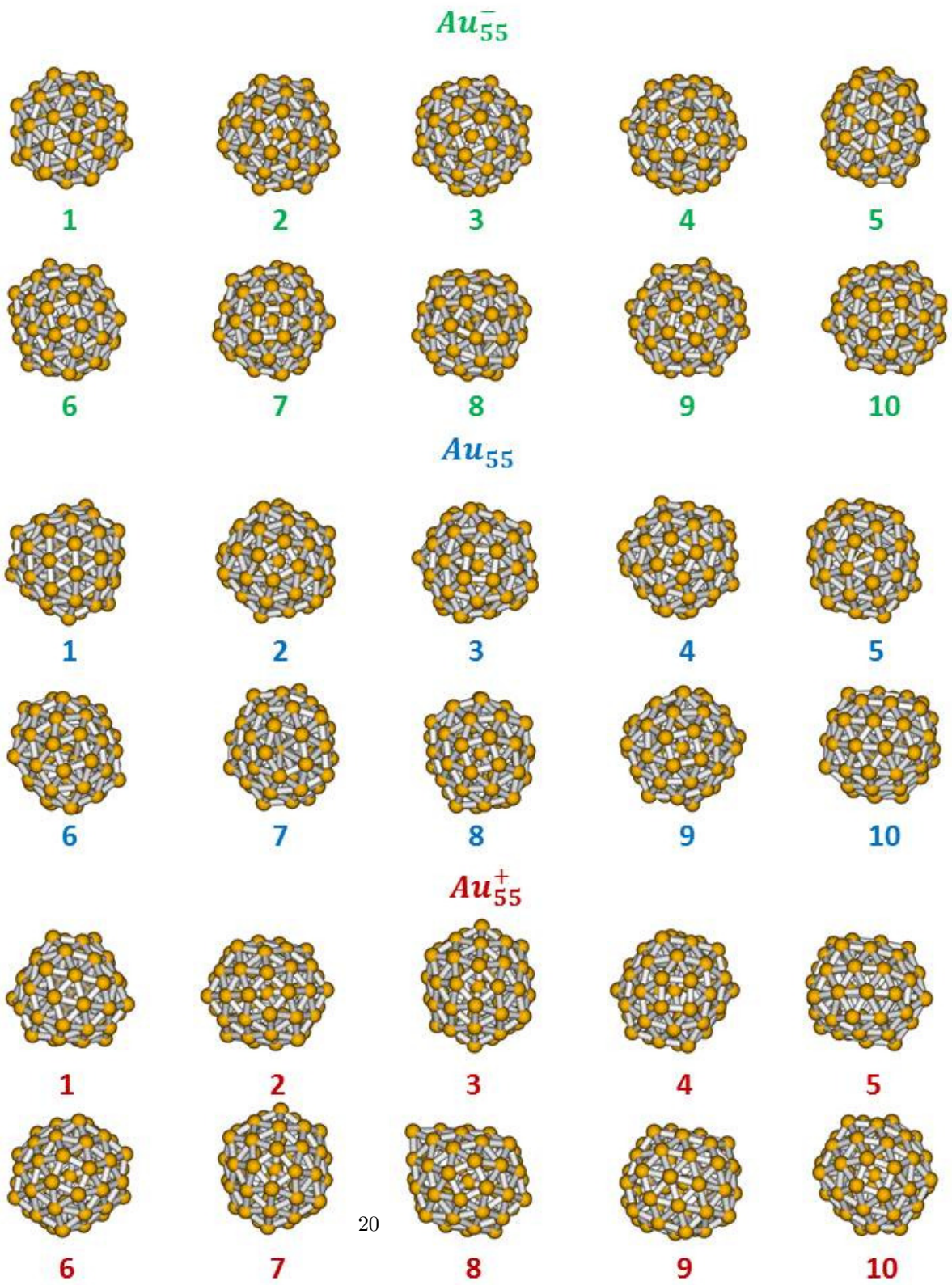

Figure 6: 10 lowest-energy minima obtained for Au_{55}^{-} (green, top), Au_{55} (blue, middle) and Au_{55}^{+} (red, bottom).

	Isomer	ΔE (eV)	I_1	I_2	I_3	Symmetry
Au_{55}^-	1	0.000	874.0	788.6	776.1	C_1
	2	0.027	876.4	792.0	774.2	C_1
	3	0.055	847.6	819.7	795.8	C_s
	4	0.083	845.4	820.0	798.1	C_s
	5	0.111	879.8	807.0	772.6	C_1
	6	0.141	882.7	804.4	770.2	C_1
	7	0.168	867.3	805.0	785.7	C_1
	8	0.196	847.4	820.4	793.7	C_1
	9	0.224	847.2	818.8	795.6	C_1
	10	0.252	876.3	811.3	777.5	C_1
Au_{55}	1	0.000	832.4	828.2	777.5	C_3 (C_1)
	2	0.053	863.0	807.9	783.9	C_1
	3	0.095	853.8	819.7	776.5	C_1
	4	0.122	854.0	818.9	778.5	C_1
	5	0.153	851.5	821.7	777.9	C_1
	6	0.186	876.6	798.5	774.8	C_1
	7	0.213	851.7	771.9	764.0	C_1
	8	0.244	880.8	798.3	771.7	C_1
	9	0.272	855.5	810.8	777.7	C_1
	10	0.300	840.8	821.6	779.7	C_1
Au_{55}^+	1	0.000	831.8	831.8	773.5	C_3
	2	0.031	832.7	829.7	772.5	C_3
	3	0.064	839.0	832.4	772.0	C_1
	4	0.093	842.7	828.7	769.3	C_1
	5	0.132	911.3	867.2	810.4	C_2
	6	0.167	843.3	834.9	769.7	C_3
	7	0.209	847.3	826.4	771.3	C_1
	8	0.240	873.7	861.7	784.1	C_1
	9	0.279	898.0	866.6	822.5	C_1
	10	0.307	847.2	830.6	771.5	D_1

Table 5: Energetics and principal mass-less moments of inertia (in Å^2) of Ag_{55} clusters.

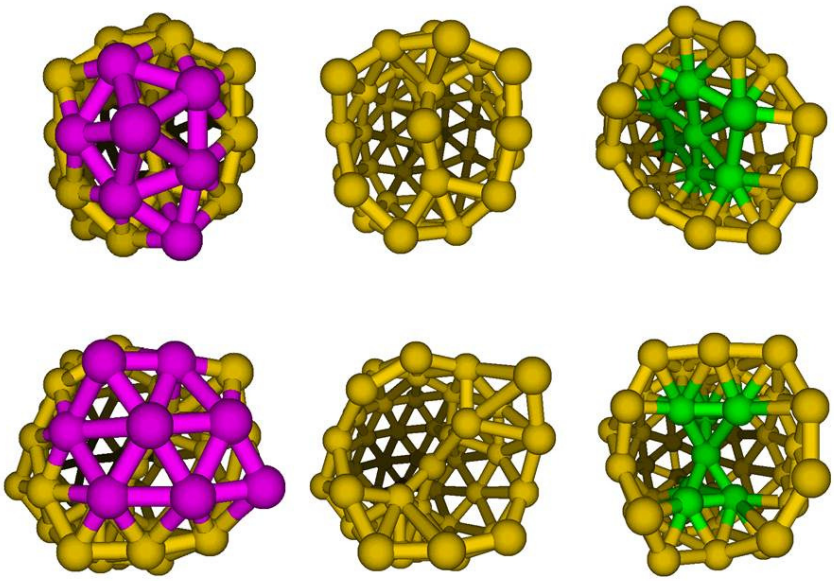

Figure 7: Perspective views of the cavities observed inside isomer number 5 of Au_{55}^{-} (top) and isomer number 5 of Au_{55}^{+} (bottom). The complete structures of the clusters are shown on the left. The violet atoms are cleared to allow for visual observation of the cavities in the middle plots. On the right plots, the clusters are oriented differently to ease the visualization of the atoms belonging to the plane (top, green) or to the pillar (bottom, green).

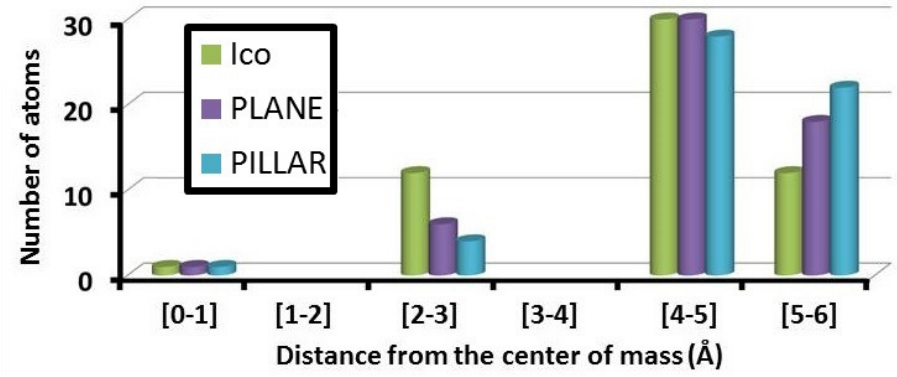

Figure 8: Radial distribution function of a 55-atom icosahedron (green), for isomer number 5 of Au_{55}^{-} (violet) (hollow structure with a separating plane) and for isomer number 5 of Au_{55}^{+} (blue) (hollow structure with a central pillar).

4. Discussion

The structure of 20-atom gold and silver clusters was addressed experimentally via several techniques. The cationic and anionic clusters were addressed in high resolution photo-electron spectroscopy experiments [35, 50, 30] and from trapped ion electron diffraction (TIED) measurements [52, 48, 53]. A very detailed analysis of the structure of ions (cations and anions) using DFT calculations combined with TIED experimental data for 20-atom metal clusters with various charges was carried out by Letchke and coworkers [53]. A review was given by Schoss et al. [83]. Assignment of the structures in those experiments generally requires an interplay with theory, and a number of *ab initio* calculations, generally in the DFT framework, have been carried out either independently or in direct combination to support the experiments [44, 35, 51, 38, 53].

Neutral Au_{20} was characterized from IR spectroscopy[39] and assigned a tetrahedral structure with high T_d symmetry, while the ions structures were probed in TIED experiments. The present lowest energy DFTB structures for Au_{20} and its ions are found to be tetrahedral-like fcc type structures. The neutral 20-mer and the cation have exact T_d symmetry, while the anion is slightly

deformed due to a Jahn-Teller distortion. In the case of neutrals, most higher energy isomers retain the fcc character, although some defects appear. In the case of the ions, the SCC-DFTB higher energy isomers display larger structural fluctuations (mixing of fcc and icosahedral patterns), and, even when similar, do not appear in the same energetic ordering as in the neutral case. The present results are in good agreement with the DFT calculations of Letchke and other authors for the lowest-energy structures of Au_{20}, Au_{20}^+ and Au_{20}^-. Note that the ionic clusters are both characterized at the DFT level by small D_{2d} distortions of the tetrahedral T_d geometry. As mentionned previously, this is also the case for the anion in the present DFTB calculation, not for the cation. For Au_{20}^-, the experimental TIED data [53] show a very good correlation with the lowest energy tetrahedral isomer and the same assignment had been found from photoelectron spectra experiments [35]. For the cationic species, a mixing between the lowest isomer and the two next ones was found to fit best the TIED data.

The situation of Ag_{20} and its ions is quite different. Most of the low energy structures found with the present SCC-DFTB scheme consist of variations around an icosahedral-like core, completed or displaying defects. In all cases, the tetrahedral structure is much higher in energy (ΔE = 0.97, 1.30 and 1.04 eV for the neutral, the cation and the anion, respectively [67]). The SCC-DFTB lowest-energy configurations of Ag_{20} and Ag_{20}^+ actually have C_3 symmetry and display very small geometrical differences as can be inferred from the principal inertia moments. In contrast, the SCC-DFTB symmetry of Ag_{20}^- is found to be C_s. The present results for the neutral are in good agreement with the DFT results of Letchke et al. [53]. They differ in the case of the anion, although the global icosahedron core pattern is the same in both calculations. Let us note that we find ten isomers for Ag_{20} in a 0.1 eV range and a similar quasi-degeneracy is found by Letchke et al. [53]. Moreover, the assignment of TIED data strongly confirmed the presence of icosahedron-core isomers, but hardly allowed for specific isomer discrimination. Let us also note the recent DFT calculations by Dhillon et al. [27] and Chen et al. [28], which, despite the use of the same TPSS functional, find different results for Ag_{20}. Indeed, the lowest

isomer of Dhillon is based on an icosahedral pattern, while that of Chen et al. displays a tetrahedral structure.

The situation is less documented for 55-atom clusters. Photo-electron spectroscopy results [38] revealed a clear structuration and a high degeneracy of the electronic energy levels in the case of Ag_{55}^-, consistent with a high symmetry shape. In contrast, the photo-electron spectrum for gold was found to be much less structured, suggesting a more intricate electronic structure, possibly corresponding to a less ordered cluster morphology, or to a mixing of structures in the experiment. Hakkinen et al. [34, 51, 38] relaxed at the DFT/LDA level selected geometries such as the icosahedron and cuboctahedron structures, or configurations originating from optimal structures generated with Morse, Sutton-Chen, Gupta and Glue potentials. They found the icosahedron to be the lowest-energy configuration in the case of Ag_{55}^- while Sutton Chen and Glue structures were the lowest ones for Au_{55}^-, the very symmetric cuboctahedral and icosahedral configurations lying at higher energy. The calculated DFT/LDA photo-electron spectra for the lowest-energy isomers of Au_{55}^- appeared to be in line with a rather disordered electronic structure, although the authors mentioned that none of them fully matched the experimental spectra, and that other structures should be considered. Schoss et al. [48] provided TIED data for Ag_{55}^+ and Ag_{55}^-, and showed their correspondence with icosahedral structures, slightly distorted in the case of the anion. The present SCC-DFTB investigation also presents very contrasted results for Ag_{55} and Au_{55}. The lowest energy structure of Ag_{55}, Ag_{55}^+ Ag_{55}^- are found to be Jahn-Teller slightly distorted I_h icosahedrons. In contrast, Au_{55} clusters offer a completely different picture. Indeed, in gold, due to the fact that the structures are more disordered, the SCC-DFTB lowest-energy isomers show a strong dependence upon the charge state. Let us mention a recent size-selected scanning transmission electron microscopy investigation of Wang and Palmer [49], who report a better correspondence of the Au_{55} STEM images with low symmetry structures *vs* icosahedra or cuboctahedra, among which possibly chiral geometries. They also report possible structures mixing ordered parts with disordered ones. Some of the higher energy isomers reported

in the present study possess such dual structure, in particular isomer Au_{55} (1). An extremely interesting finding is that many isomers of Au_{55} reported in the present study are less compact than those of silver and display cavities, and even sometimes multiple cavities, below the external shell. The possibilities for gold clusters to exhibit cage patterns have already been mentioned in a number of theoretical studies, in particular for Au_{16}^{2-} and Au_{34}^{2-}, and also for various clusters in the range 32-56 [84]. However, all previous studies did rely on DFT relaxation of *a priori* cage guesses, and not from a global optimization scheme. Thus, to the best of our knowledge, it is the first time that cavities are obtained directly from a global optimization procedure without *a priori* constraints for clusters in this size range. In order to check the stability of such cavity displaying structure, DFT calculations have been achieved (PW91[85]/PAW[86, 87], see supplementary material for computational details). We present in table 4 the relative stability of selected Au_{55} structures, including the most stable isomer (Au_{55}, isomer 1) obtained in this work and various structures reported in reference [51]. Table 4 shows that isomer 1 is stable and remains the most stable structure at the DFT level. The DFT and DFTB energetic orderings of the isomers are similar. The cavity structure (isomer 1) is particularly stable at the DFTB level, which explains the largest structural excitation energies of the other isomers. Note that Morse and Icosahedron structures experienced significant geometrical changes in the DFT relaxation leading, respectively, to internal cavities or local surface concavities. The latter being also observed in the DFTB relaxation of the Icosahedron structure.

One may also analyze the characteristics of the density of isomers from the present calculations. It is seen that in the case of highly symmetric or quasi-symmetric minimal energy isomers (such as the quasi-tetrahedral or quasi-icosahedral), the gaps between the SCC-DFTB absolute minima and the second isomers are larger than for less symmetric structures. This is for instance the case for Au_{20} ($\Delta E = 0.694$ eV) *vs* Ag_{20} ($\Delta E = 0.119$ eV). The same trend can be observed for Ag_{55} ($\Delta E = 0.509$ eV) *vs* Au_{55} ($\Delta_E = 0.053$ eV). The addition or removal of an electron causes a lowering of this structural energy gap and,

Structure	DFT/PW91/PAW	DFTB
Cuboctahedron	3.073	5.14
Decahedron	2.429	4.91
Icosahedron	1.587*	4.36*
Glue	1.574	3.66
Sutton-Chen	1.110	3.33
Morse	0.394*	3.37
Isomer 1, this work	0	0

Table 6: DFT and DFTB structural excitation energies (eV) for a sample of selected Au_{55} structures taken from the present work and from ref. [51]. * indicates a significant structural variation during the optimization.

in general, an increase of the density of isomers. This can also be inferred from Table 1 at least for the 20-atom clusters. It is worth mentioning that in the case of the 20-atom clusters, the present SCC-DFTB isomer gaps are in quite good agreement with the DFT results of Letchke et al. [53].

Finally, Figure 5 shows a clear difference in the cumulative coordination numbers of the ten isomers investigated here for Ag_{55} and Au_{55}. A bi-modal distance distribution is observed in the case of silver in contrast to gold which is characterized by a much broader distribution. This somewhat quantifies the order difference between 55-atom gold and silver clusters, not only for the minimal energy structures, but also for the next low-lying isomers.

5. Conclusion

There are several conclusions and perspectives to the present study: (i) It demonstrates the feasibility of global optimization using DFTB without pre-screening involving a classical potential for sizes up to a few tens of atoms. DFTB is in particular able to deal with Jahn-Teller distorsions; (ii) It proves that the DFTB structures obtained are consistent with previous calculations and available experimental assignments for Au_{20}, Ag_{20} or Ag_{55} ions. It is also in

qualitative agreement with the photo-electron detachment experiments, TIED experiments and previous calculations based on relaxation of pre-selected configurations for Ag_{55}^- and Au_{55}^-. If the nearly icosahedral character of the structures of Ag_{55} and its ions seems now to be well grounded, final conclusion in the case of gold will require further investigations due to larger structural disorder. The present DFTB calculations reveal new disordered structures which have not been previously reported, and may be consistent with the experimental findings in the case of Au_{55}. We have validated the stability of the lowest energy Au_{55} isomer (cavity type), using a DFT+GGA functional. Obviously, this validation should be further credited by means of DFT with high level functionals and by the calculation of the experimentally measured observables. This is however beyond the scope of the present work; (iii) The present investigation opens direct perspectives such as unbiased optimization addressing other interesting sizes (cages) and a range which covers the transition between clusters and nanoparticles, but also multiply charged clusters; (iv) Finally it will be extremely convenient to use DFTB to investigate phase changes and thermodynamical properties of noble metal clusters.

6. Appendix A. Supplementary material

Supplementary data associated with this article can be found, in the online version, at XXX . It contains details about DFT computational details, energetics, structural properties and cartesian coordinates of the DFTB isomers.

7. Acknowledgements

This work was granted access to the HPC resources of CALMIP (Grants p1303 and p0059) and from IDRIS (Grant i2015087375). It was supported by a CNRS-Inphyniti Grant (ATHENA 2015 project), the CNRS-GDR EMIE and the NEXT grants ANR-10-LABX-0037 in the framework of the *Programme des Investissements d'Avenir* (CIM3 and EXTAS projects).

References

[1] V. Kasperovich, V. V. Kresin, Ultraviolet photoabsorption spectra of silver and gold nanoclusters, Philos. Mag. B 78 (4) (1998) 385–396.

[2] S. Lecoultre, A. Rydlo, C. Felix, J. Buttet, S. Gilb, W. Harbich, Optical absorption of small copper clusters in neon: Cu_n, (n = 1–9), J. Chem. Phys. 134 (7) (2011) 074303.

[3] V. E. Kaydashev, E. Janssens, P. Lievens, Optical absorption spectra of palladium doped gold cluster cations, J. Chem. Phys. 142 (3) (2015) 034310.

[4] B. Anak, M. Bencharif, F. Rabilloud, Time-dependent density functional study of uv-visible absorption spectra of small noble metal clusters (cu_n, ag_n, au_n, n = 2-9, 20), RSC Adv. 4 (2014) 13001–13011.

[5] M. Harb, F. Rabilloud, D. Simon, A. Rydlo, S. Lecoultre, F. Conus, V. Rodrigues, C. Felix, Optical absorption of small silver clusters: Ag_n, (n=4-22), J. Chem. Phys. 129 (19) (2008) 194108.

[6] C.-C. Huang, Z. Yang, K.-H. Lee, H.-T. Chang, Synthesis of highly fluorescent gold nanoparticles for sensing mercury(ii), Angew. Chem., Int. Ed. 46 (36) (2007) 6824–6828.

[7] H. Xu, K. S. Suslick, Water-soluble fluorescent silver nanoclusters, Adv. Mater. 22 (10) (2010) 1078–1082.

[8] Z. Wu, R. Jin, On the ligand's role in the fluorescence of gold nanoclusters, Nano Lett. 10 (7) (2010) 2568–2573.

[9] W. Harbich, S. Fedrigo, J. Buttet, The optical absorption spectra of small silver clusters (n=5–11) embedded in argon matrices, Chemical Physics Letters 195 (5) (1992) 613 – 617. doi:http://dx.doi.org/10.1016/0009-2614(92)85572-R.
URL http://www.sciencedirect.com/science/article/pii/0009261492855 72R

[10] S. Fedrigo, W. Harbich, J. Buttet, Collective dipole oscillations in small silver clusters embedded in rare-gas matrices, Phys. Rev. B 47 (1993) 10706–10715. doi:10.1103/PhysRevB.47.10706.
URL http://link.aps.org/doi/10.1103/PhysRevB.47.10706

[11] Tabarin, T., Antoine, R., Compagnon, I., Broyer, M., Dugourd, P., Mitrić, R., Petersen, J., Bonačić-Koutecký, V., Eur. Phys. J. D (1). doi:10.1140/epjd/e2007-00118-5.

[12] K. Baishya, J. C. Idrobo, S. Öğüt, M. Yang, K. Jackson, J. Jellinek, Optical absorption spectra of intermediate-size silver clusters from first principles, Phys. Rev. B 78 (2008) 075439. doi:10.1103/PhysRevB.78.075439.
URL http://link.aps.org/doi/10.1103/PhysRevB.78.075439

[13] G.-T. Bae, C. M. Aikens, Tddft and cis studies of optical properties of dimers of silver tetrahedra, The Journal of Physical Chemistry A 116 (31) (2012) 8260–8269. doi:10.1021/jp305330e.
URL http://dx.doi.org/10.1021/jp305330e

[14] G. M. Koretsky, M. B. Knickelbein, The reactions of silver clusters with ethylene and ethylene oxide: Infrared and photoionization studies of $ag_n(c_2h_4)_m$, $ag_n(c_2h_4o)_m$ and their deuterated analogs, J. Chem. Phys. 107 (24) (1997) 10555–10566.

[15] M. Valden, X. Lai, D. W. Goodman, Onset of catalytic activity of gold clusters on titania with the appearance of nonmetallic properties, Science 281 (5383) (1998) 1647–1650.

[16] N. Lopez, J. K. Norskov, Catalytic co oxidation by a gold nanoparticle: a density functional study, J. Am. Chem. Soc. 124 (38) (2002) 11262–11263.

[17] L. M. Molina, B. Hammer, Active role of oxide support during co oxidation at au/mgo, Phys. Rev. Lett. 90 (2003) 206102.

[18] S. Chretien, M. S. Gordon, H. Metiu, Density functional study of the adsorption of propene on silver clusters, $ag_m^q(m = 1-5; q = 0, +1)$, J. Chem. Phys. 121 (20) (2004) 9925–9930.

[19] S. Klacar, A. Hellman, I. Panas, H. Gronbeck, Oxidation of small silver clusters: a density functional theory study, J. Phys. Chem. C 114 (29) (2010) 12610–12617.

[20] A. H. Larsen, J. Kleis, K. S. Thygesen, J. K. Norskov, K. W. Jacobsen, Electronic Shell Structure and Chemisorption on Gold Nanoparticles, Phys. Rev. B 84 (24) (2011) 245429.

[21] L. D. Socaciu, J. Hagen, J. Le Roux, D. Popolan, T. M. Bernhardt, L. Wöste, Š. Vajda, Strongly cluster size dependent reaction behavior of co with o2 on free silver cluster anions, The Journal of Chemical Physics 120 (5) (2004) 2078–2081.
URL http://scitation.aip.org/content/aip/journal/jcp/120/5/10.1063/1.1644103

[22] A. Fielicke, P. Gruene, G. Meijer, D. M. Rayner, The adsorption of {CO} on transition metal clusters: A case study of cluster surface chemistry, Surface Science 603 (10–12) (2009) 1427 – 1433, special Issue of Surface Science dedicated to Prof. Dr. Dr. h.c. mult. Gerhard Ertl, Nobel-Laureate in Chemistry 2007. doi:http://dx.doi.org/10.1016/j.susc.2008.09.064.
URL http://www.sciencedirect.com/science/article/pii/S0039602809000636

[23] R. Fournier, Theoretical Study of the Structure of Silver Clusters, J. Chem. Phys. 115 (5) (2001) 2165–2177.

[24] E. Fernández, J. Soler, I. Garzón, L. Balbás, Trends in the Structure and Bonding of Noble Metal Clusters, Phys. Rev. B 70 (16) (2004) 165403.

[25] M. Pereiro, D. Baldomir, Determination of the lowest-energy structure of ag_8 from first-principles calculations, Phys. Rev. A 72 (2005) 045201.

[26] M. Yang, K. A. Jackson, J. Jellinek, First-principles study of intermediate size silver clusters: Shape evolution and its impact on cluster properties, J. Chem. Phys. 125 (14) (2006) 144308.

[27] H. Dhillon, R. Fournier, Geometric Structure of Silver Clusters with and Without Adsorbed Cl and Hg, Comput. Theor. Chem. 1021 (2013) 26–34.

[28] M. Chen, J. E. Dyer, K. Li, D. A. Dixon, Prediction of structures and atomization energies of small silver clusters, $(ag)_n$, n ¡ 100, J. Phys. Chem. A 117 (34) (2013) 8298–8313.

[29] F. Rabilloud, D. Simon, A. Rydlo, S. Lecoultre, F. Conus, V. Rodrigues, Optical absorption of small silver clusters: Ag_n (n=4-22), J. Chem. Phys. 129 (19) (2008) 194108.

[30] B. Yoon, P. Koskinen, B. Huber, O. Kostko, B. von Issendorff, H. Häkkinen, M. Moseler, U. Landman, Size-dependent structural evolution and chemical reactivity of gold clusters, ChemPhysChem 8 (1) (2007) 157–161.

[31] X.-B. Li, H.-Y. Wang, X.-D. Yang, Z.-H. Zhu, Y.-J. Tang, Size dependence of the structures and energetic and electronic properties of gold clusters, J. Chem. Phys. 126 (8) (2007) 084505.

[32] A. V. Walker, Structure and energetics of small gold nanoclusters and their positive ions, J. Chem. Phys. 122 (9) (2005) 094310.

[33] H. Häkkinen, U. Landman, Gold clusters (au_n, $2 \leq n \leq 10$) and their anions, Phys. Rev. B 62 (2000) 2287–2290.

[34] H. Häkkinen, M. Moseler, U. Landman, Bonding in cu, ag, and au clusters: Relativistic effects, trends, and surprises, Phys. Rev. Lett. 89 (2002) 033401.

[35] H. Häkkinen, B. Yoon, U. Landman, X. Li, H.-J. Zhai, L.-S. Wang, On the electronic and atomic structures of small au_n^- (n=4–14) clusters: A

photoelectron spectroscopy and density-functional study, J. Phys. Chem. A 107 (32) (2003) 6168–6175.

[36] L. Xiao, L. Wang, From planar to three-dimensional structural transition in gold clusters and the spin–orbit coupling effect, Chem. Phys. Lett. 392 (2004) 452–455.

[37] L. Xiao, B. Tollberg, X. Hu, L. Wang, Structural study of gold clusters, J. Chem. Phys. 124 (11) (2006) 114309.

[38] H. Häkkinen, Atomic and electronic structure of gold clusters: Understanding flakes, cages and superatoms from simple concepts, Chem. Soc. Rev. 37 (2008) 1847–1859.

[39] P. Gruene, D. M. Rayner, B. Redlich, A. F. G. van der Meer, J. T. Lyon, G. Meijer, A. Fielicke, Structures of neutral au_7, au_{19}, and au_{20} clusters in the gas phase, Science 321 (5889) (2008) 674–676.

[40] M. P. Johansson, A. Lechtken, D. Schooss, M. M. Kappes, F. Furche, 2d-3d transition of gold cluster anions resolved, Phys. Rev. A 77 (2008) 053202.

[41] A. Lechtken, C. Neiss, J. Stairs, D. Schooss, Comparative study of the structures of copper, silver, and gold icosamers: Influence of metal type and charge state, J. Chem. Phys. 129 (15) (2008) 154304.

[42] W. Huang, S. Bulusu, R. Pal, X. C. Zeng, L.-S. Wang, Structural transition of gold nanoclusters: From the golden cage to the golden pyramid, ACS Nano 3 (5) (2009) 1225–1230.

[43] R. Pal, L.-M. Wang, W. Huang, L.-S. Wang, X. C. Zeng, Structure evolution of gold cluster anions between the planar and cage structures by isoelectronic substitution: Au_n^- (n = 13–15) and mau_n^- (n = 12–14; m = ag, cu), J. Chem. Phys. 134 (5) (2011) 054306.

[44] V. Bonačić-Koutecký, J. Burda, R. Mitrić, M. Ge, G. Zampella, P. Fantucci, Density functional study of structural and electronic properties

of bimetallic silver–gold clusters: Comparison with pure gold and silver clusters, The Journal of Chemical Physics 117 (7) (2002) 3120–3131.
URL http://scitation.aip.org/content/aip/journal/jcp/117/7/10.1063/1.1492800

[45] F. Furche, R. Ahlrichs, P. Weis, C. Jacob, S. Gilb, T. Bierweiler, M. M. Kappes, The structures of small gold cluster anions as determined by a combination of ion mobility measurements and density functional calculations, J. Chem. Phys. 117 (15) (2002) 6982–6990.

[46] M. P. Johansson, I. Warnke, A. Le, F. Furche, At what size do neutral gold clusters turn three-dimensional?, J. Phys. Chem. C 118 (50) (2014) 29370–29377.

[47] A. Tanwar, E. Fabiano, E. P. Trevisanutto, L. Chiodo, F. Della Sala, Accurate ionization potential of gold anionic clusters from density functional theory and many-body perturbation theory, Eur. Phys. J. B 86 (4) (2013) 161.

[48] D. Schooss, M. N. Blom, J. H. Parks, B. v. Issendorff, H. Haberland, M. M. Kappes, The structures of ag55+ and ag55-: Trapped ion electron diffraction and density functional theory, Nano Letters 5 (10) (2005) 1972–1977. doi:10.1021/nl0513434.
URL http://dx.doi.org/10.1021/nl0513434

[49] Z. W. Wang, R. E. Palmer, Experimental evidence for fluctuating, chiral-type au55 clusters by direct atomic imaging, Nano Letters 12 (11) (2012) 5510–5514. doi:10.1021/nl303429z.
URL http://dx.doi.org/10.1021/nl303429z

[50] J. Li, X. Li, H.-J. Zhai, L.-S. Wang, Au_20: A tetrahedral cluster, Science 299 (5608) (2003) 864–867.

[51] H. Häkkinen, M. Moseler, O. Kostko, N. Morgner, M. A. Hoffmann, B. v. Is-

sendorff, Symmetry and electronic structure of noble-metal nanoparticles and the role of relativity, Phys. Rev. Lett. 93 (9) (2004) 093401.

[52] X. Xing, B. Yoon, U. Landman, J. H. Parks, Structural evolution of au nanoclusters: From planar to cage to tubular motifs, Physical Review B 74 (16) (2006) 165423–.
URL http://link.aps.org/doi/10.1103/PhysRevB.74.165423

[53] A. Lechtken, C. Neiss, J. Stairs, D. Schooss, Comparative study of the structures of copper, silver, and gold icosamers: Influence of metal type and charge state, The Journal of Chemical Physics 129 (15) (2008) 154304.
URL http://scitation.aip.org/content/aip/journal/jcp/129/15/10.1063/1.2992073

[54] D. Porezag, T. Frauenheim, T. Köhler, G. Seifert, R. Kaschner, Construction of tight-binding-like potentials on the basis of density-functional theory: Application to carbon, Phys. Rev. B 51 (1995) 12947–12957.

[55] G. Seifert, D. Porezag, T. Frauenheim, Calculations of molecules, clusters, and solids with a simplified lcao-dft-lda scheme, Int. J. Quantum Chem. 58 (1996) 185–192.

[56] M. Elstner, D. Porezag, G. Jungnickel, J. Elsner, M. Haugk, T. Frauenheim, S. Suhai, G. Seifert, Self-consistent-charge density-functional tight-binding method for simulations of complex materials properties, Phys. Rev. B 58 (1998) 7260–7268.

[57] T. Frauenheim, G. Seifert, M. Elsterner, Z. Hajnal, G. Jungnickel, D. Porezag, S. Suhai, R. Scholz, A self-consistent charge density-functional based tight-binding method for predictive materials simulations in physics, chemistry and biology, Phys. Status Solidi B 217 (2000) 41–62.

[58] T. Frauenheim, G. Seifert, M. Elstner, T. Niehaus, C. Köhler, M. Amkreutz, M. Sternberg, Z. Hajnal, A. D. Carlo, S. Suhai, Atomistic

simulations of complex materials: Ground-state and excited-state properties, J. Phys.: Condens. Matter 14 (2002) 3015–3047.

[59] A. Oliveira, G. Seifert, T. Heine, H. Duarte, Density-functional based tight-binding: an approximate dft method, J. Braz. Chem. Soc. 20 (2009) 1193–1205.

[60] L. F. L. Oliveira, J. Cuny, M. Moriniere, L. Dontot, A. Simon, F. Spiegelman, M. Rapacioli, Phase changes of the water hexamer and octamer in the gas phase and adsorbed on polycyclic aromatic hydrocarbons, Phys. Chem. Chem. Phys. 17 (2015) 17079–17089.

[61] M. Rapacioli, A. Simon, L. Dontot, F. Spiegelman, Extensions of dftb to investigate molecular complexes and clusters, physica status solidi (b) 249 (2) (2012) 245–258. doi:10.1002/pssb.201100615.
URL http://dx.doi.org/10.1002/pssb.201100615

[62] T. H. Choi, Simulation of the $(h_2o)_8$ cluster with the scc-dftb electronic structure method, Chem. Phys. Lett. 543 (2012) 45–49.

[63] L. Dontot, N. Suaud, M. Rapacioli, F. Spiegelman, An extended dftb-ci model for charge-transfer excited states in cationic molecular clusters: Model studies versus ab initio calculations in small pah clusters, Phys. Chem. Chem. Phys. 18 (2016) 3545–3557.

[64] A. Fihey, C. Hettich, J. Touzeau, F. Maurel, A. Perrier, C. Köhler, B. Aradi, T. Frauenheim, Scc-dftb parameters for simulating hybrid gold-thiolates compounds, J. Comput. Chem. 36 (27) (2015) 2075–2087.

[65] P. Koskinen, H. Häkkine, G. Seifert, S. Sanna, T. Frauenheim, M. Moseler, Density-functional based tight-binding study of small gold clusters, New J. Phys. 8 (1) (2006) 9.

[66] B. Szűcs, Z. Hajnal, R. Scholz, S. Sanna, T. Frauenheim, Theoretical study of the adsorption of a ptcda monolayer on s-passivated gaas(1 0 0), Appl. Surf. Sci. 234 (1–4) (2004) 173–177.

[67] L. F. L. Oliveira, N. Tarrat, J. Cuny, J. Morillo, D. Lemoine, F. Spiegelman, M. Rapacioli, Benchmarking density functional based tight-binding for silver and gold materials: From small clusters to bulk, The Journal of Physical Chemistry A 120 (42) (2016) 8469–8483. doi:10.1021/acs.jpca.6b09292.
URL http://dx.doi.org/10.1021/acs.jpca.6b09292

[68] P. Hohenberg, W. Kohn, Inhomogeneous electron gas, Phys. Rev. 136 (3B) (1964) B864–B871.
URL http://link.aps.org/doi/10.1103/PhysRev.136.B864

[69] W. Kohn, L. J. Sham, Self-consistent equations including exchange and correlation effects, Phys. Rev. 140 (4A) (1965) A1133–A1138.
URL http://link.aps.org/doi/10.1103/PhysRev.140.A1133

[70] Z. Li, H. A. Scheraga, Monte carlo-minimization approach to the multiple-minima problem in protein folding, Proceedings of the National Academy of Sciences 84 (19) (1987) 6611–6615.
URL http://www.pnas.org/content/84/19/6611.abstract

[71] D. J. Wales, J. P. K. Doye, Global optimization by basin-hopping and the lowest energy structures of lennard-jones clusters containing up to 110 atoms, The Journal of Physical Chemistry A 101 (28) (1997) 5111–5116. doi:10.1021/jp970984n.
URL http://dx.doi.org/10.1021/jp970984n

[72] S. Kirkpatrick, C. D. Gelatt, M. P. Vecchi, Optimization by simulated annealing, Science 220 (4598) (1983) 671–680.

[73] Y. Sugita, Y. Okamoto, Replica-exchange molecular dynamics method for protein folding, Chem. Phys. Lett. 314 (1-2) (1999) 141–151.

[74] R. H. Swendsen, J.-S. Wang, Replica monte carlo simulation of spin-glasses, Physical Review Letters 57 (21) (1986) 2607–2609.
URL http://link.aps.org/doi/10.1103/PhysRevLett.57.2607

[75] D. E. Goldberg, Genetic Algorithms in Search, Optimization and Machine Learning, Addison-Wesley Longman Publishing Co., Inc., 1989.

[76] J. Kennedy, R. Eberhart, Particle swarm optimization, Proc. of IEEE int. conf. on neural networks 4 (1995) 1942–1948.

[77] S. Nosé, A unified formulation of the constant temperature molecular dynamics methods, J. Chem. Phys. 81 (1) (1984) 511. doi:10.1063/1.447334.
URL http://scitation.aip.org/content/aip/journal/jcp/81/1/10.1063/1.447334

[78] W. G. Hoover, Canonical dynamics: Equilibrium phase-space distributions, Phys. Rev. A 31 (3) (1985) 1695–1697.

[79] T. Heine, M. Rapacioli, S. Patchkovskii, J. Cuny, J. Frenzel, A. Koster, P. Calaminici, H. A. Duarte, S. Escalante, R. Flores-Moreno, A. Goursot, J. Reveles, D. Salahub, A. Vela, deMonNano, http://demon-nano.ups-tlse.fr/, 1st Sept 2016 (2015).

[80] A. F. Oliveira, P. Philipsen, T. Heine, Dftb parameters for the periodic table, part 2: Energies and energy gradients from hydrogen to calcium, J. Chem. Theory Comput. 11 (11) (2015) 5209–5218.

[81] L. Vázquez-Vidal, Molsym: A program on molecular symmetry and group theory, Journal of Chemical Education 73 (4) (1996) 321. doi:10.1021/ed073p321.
URL http://dx.doi.org/10.1021/ed073p321

[82] P. Pyykko, Relativistic effects in structural chemistry, Chem. Rev. 88 (3) (1988) 563–594.

[83] D. Schooss, P. Weis, O. Hampe, M. M. Kappes, Determining the size-dependent structure of ligand-free gold-cluster ions, Philosophical Transactions of the Royal Society A: Mathematical, Physical and Engineering Sciences 368 (1915) (2010) 1211–1243.

[84] J. Wang, J. Jellinek, J. Zhao, Z. Chen, R. B. King, P. von RaguéSchleyer, Hollow cages versus space-filling structures for medium-sized gold clusters: The spherical aromaticity of the au50 cage, The Journal of Physical Chemistry A 109 (41) (2005) 9265–9269. doi:10.1021/jp052414q.
URL http://dx.doi.org/10.1021/jp052414q

[85] J. P. Perdew, J. A. Chevary, S. H. Vosko, K. A. Jackson, M. R. Pederson, D. J. Singh, C. Fiolhais, Atoms, molecules, solids, and surfaces: Applications of the generalized gradient approximation for exchange and correlation, Phys. Rev. B 46 (1992) 6671–6687. doi:10.1103/PhysRevB.46.6671.
URL http://link.aps.org/doi/10.1103/PhysRevB.46.6671

[86] P. E. Blöchl, Projector augmented-wave method, Physical Review B 50 (24) (1994) 17953–17979.
URL http://link.aps.org/doi/10.1103/PhysRevB.50.17953

[87] G. Kresse, D. Joubert, From ultrasoft pseudopotentials to the projector augmented-wave method, Physical Review B 59 (3) (1999) 1758–1775.
URL http://link.aps.org/doi/10.1103/PhysRevB.59.1758